Int J Thermophys (2009) 30:648–660
DOI 10.1007/s10765-008-0548-0

A Model for the Hybridization Exothermic Effect in Label-Free Biodetections by a Nanomechanical Cantilever-DNA Chip

Neng-Hui Zhang · Jian-Zhong Chen · Shu-Xiao Wan

Received: 12 April 2008 / Accepted: 24 November 2008 / Published online: 30 December 2008

Abstract The influence of the hybridization exothermic effect on nanomechanical deflections of DNA chips in label-free biodetections is investigated. First, from the related experimental curves, the thermal variation of the biolayer during the linkage of DNA base pairs is estimated by Breslauer's method and the Langmuir adsorption isotherm. Second, the temperature field of the chip is obtained by the lumped parameter model and the classical Fourier's method. Third, the nanomechanical deflection of the chip is predicted by an alternative model for thermoelastic problems of laminated cantilever beams. The effect of a DNA base sequence on thermal deflection of chips is also investigated. In the case of adiabatic conditions, numerical results show that the theoretical predicted value of 1.5 nm to 2 nm deflection is within the scope of the optical-beam-deflection readout system's accuracy.

Keywords Cantilever-DNA chip · Hybridization exothermic effect · Langmuir adsorption isotherm · Lumped parameter method · Nanomechanics

1 Introduction

In recent years, microcantilever-based biosensors have attracted much attention [1–10]. The low-cost sensors not only show fast response, high sensitivity, and suitability for parallelization into arrays [11] but also provide common platforms for

N.-H. Zhang (✉)
Department of Mechanics, College of Sciences, Shanghai University,
No. 99 Shangda Road, Shanghai 200444, China
e-mail: nhzhang@shu.edu.cn

N.-H. Zhang · J.-Z. Chen · S.-X. Wan
Shanghai Institute of Applied Mathematics and Mechanics,
Shanghai University, Shanghai 200072, China

label-free analysis such as DNA hybridization, antigen–antibody binding, and drug discovery.

Experiments reveal that the chip deflection can arise from numerous factors, such as salt concentration in buffer solution [9], concentration [10], length and sequence [5] of DNA molecules, grafting density, and hybridization density [4], time, temperature, etc. The deflection is measured by a single- or multiple-point optical deflection technique [12].

A number of bending mechanisms were proposed to explain the origin of nanomechanical cantilever motion generated from chemo-mechanical interactions between adsorbed biomolecules and substrates, but they are the subject of great controversy in the scientific community. Based on different experiments in different conditions, they are attributed to surface stress [4–6,10,13], surface energy [14], configurational entropy and intermolecular energetics [9], physical steric crowding [8], the covalent attachment to the gold surface [6], the curvature electricity effect of biomembrane [7,15], or the piezoelectric effect of biolayer [2,3]. Obviously, many discrepancies slow the advance of the application of this new technology. This also draws more attention to this new area.

When the temperature changes, bimaterial microcantilevers undergo bending due to dissimilar thermal expansion of two different materials composing the cantilever. This phenomenon is frequently referred to as the "bimetallic effect" [16,17]. The biochip is actually a microcantilever-laminated structure made of a single- or double-stranded DNA (ssDNA or dsDNA) biolayer and three non-biolayers. In addition, there exist various noises, including thermomechanical noise, Nyquist–Johnson noise, adsorption–desorption noise, defect motion-induced noise, etc. [18]. So the bimetallic effect is inevitable in the label-free biodetection process. A fast relaxation process was observed during the hybridization process [10], which is assigned to bimetallic effects arising from a slightly different temperature of the injected sample solution compared to that of the buffer in the liquid cell. Usually, the deflection induced by thermal drifts can be eliminated by the differential deflection technique. In fact, the use of microcantilever arrays enables detection of several analyses simultaneously and solves the inherent problem of thermal drift often present when using single microcantilever sensors, as some of the cantilevers can be used as sensor cantilevers for detection and other cantilevers serve as passivated reference cantilevers that do not exhibit affinity to the molecules to be detected. However, experimental studies [11] revealed that only about 40 % of the cantilevers fell into the "tracking" category, where the drift of the cantilevers was correlated for periodic temperature cycles. This indicates that the differential deflection technique is not applicable to "non-tracking" cantilevers, especially for dynamic modes.

Besides temperature fluctuations in the background, there is also a temperature fluctuation induced by biochemical reactions during hybridization processes. Titration, differential scanning calorimetry, and van't Hoff analysis of ultraviolet (UV) thermal scanning experiments [19,20] showed that heat loss exists in the formation of an oligomeric DNA duplex. So, the hybridization process is exothermic. The variation of free energy depends on a DNA chain's base sequence. More specifically, it depends primarily on the identity of the nearest-neighbor bases. Ten different nearest-neighbor interactions are possible in any Watson–Crick DNA duplex structure. These pairwise

interactions are AA/TT, AT/TA, TA/AT, CA/GT, GT/CA, CT/GA, GA/CT, CG/GC, GC/CG, GG/CC. Breslauer et al. [19] presented a method to predict the free-energy change in the formation of DNA duplex structures by the sum of its nearest-neighbor thermodynamic experimental data. These predicted values are in excellent agreement with the corresponding values determined experimentally. However, up to now, related studies on the hybridization exothermic effect in the chip technology area are not available in the literature.

Different from previous nanomechanical models [1,21] and piezoelectric models [2,3], this article is devoted to prediction of nanomechanical deflections for DNA chips induced by the hybridization exothermic effect in label-free biodetections. First, Breslauer's nearest-neighbor method [19] is used to predict the heat loss in association of two complementary ssDNA chains. The total heat of the biolayer generated during hybridization depends on the packing density and hybridization efficiency. The amount of hybridization DNA molecules can be simulated by the Langmuir adsorption isotherm. So by the above predictions and the related experimental curves [8], the time history of the thermal variation of the biolayer is obtained. Second, three models, including the three-layer Au–Ti–Si-beam model, the single-layer Si-beam model and the lumped parameter model are used to predict the temperature field of the chip. Considering the good thermal conductivity of the Au-layer and the limitation of detection time, the heat loss to the surroundings is neglected. This means that the heat loss of the biolayer is fully adsorbed by the non-biolayers. Third, Zhang's two-variable method [22–25] for thermoelastic problems of laminated cantilever beams is used to predict the nanomechanical deflection of the chip. The effect of a DNA base sequence on thermal deflection of the chip is also investigated.

2 Mathematical Model

As shown in Fig. 1, a DNA chip with length l and width b consists of a Au/Ti/ Si-layer with individual thickness h_i ($i = 1, 2, 3$) and a DNA-layer immobilized by self-assembly technology of the thiol group. The interface between the Au-layer and the biolayer is taken as the coordinate axis x. The thermoelastic properties of the non-biolayers are $E_i, \alpha_i, k_i, \lambda_i, \rho_i, c_i$, where E is Young's modulus, α is the thermal expansion coefficient, k is the thermal diffusivity, λ is the thermal conductivity, ρ is the density, and

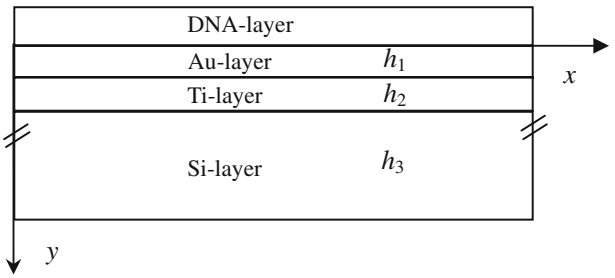

Fig. 1 Longitudinal section of a DNA chip and its coordinate system

Table 1 Thermodynamic data of the nearest-neighbor free-energy variation (kcal · mol^{-1})

First nucleotide	Second nucleotide			
	dA	dC	dG	dT
dA	−1.9	−1.3	−1.6	−1.5
dC	−1.9	−3.1	−3.6	−1.6
dG	−1.6	−3.1	−3.1	−1.3
dT	−1.0	−1.6	−1.9	−1.9

c is the specific heat capacity. Here and after, the subscripts 1, 2, 3 represent the Au/Ti/Si-layers, respectively.

2.1 Thermal Output of the Biolayer

Related experimental and theoretical studies [19,20] indicate that the free-energy variation during formation of a DNA duplex structure can be estimated by the sum of the nearest-neighbor thermodynamic interactions. The nearest-neighbor free-energy variation data are obtained experimentally and listed in Table 1 [26]. For example, when a thiolated probe DNA sequence ACATTGTCGCAA hybridizes with its complementary target DNA sequence TTGCGACAATGT, the free-energy loss is predicted as

$$\begin{aligned}\Delta G(\mathrm{ACATTGTCGCAA}) &= \Delta G(\mathrm{AC}) + \Delta G(\mathrm{CA}) + \Delta G(\mathrm{AT}) + \Delta G(\mathrm{TT}) \\ &\quad + \Delta G(\mathrm{TG}) + \Delta G(\mathrm{GT}) + \Delta G(\mathrm{TC}) + \Delta G(\mathrm{CG}) \\ &\quad + \Delta G(\mathrm{GC}) + \Delta G(\mathrm{CA}) + \Delta G(\mathrm{AA}) \\ &= -(1.3 + 1.9 + 1.5 + 1.9 \\ &\quad + 1.9 + 1.3 + 1.6 + 3.6 + 3.1 + 1.9 + 1.9) \\ &= -21.9\,\mathrm{kcal \cdot mol^{-1}} \end{aligned} \tag{1}$$

So, the thermal output during the formation of a single-DNA duplex chain is given as

$$Q_\mathrm{s} = \Delta G / N_0, \tag{2}$$

in which N_0 ($= 6.02252 \times 10^{23}$) represents Avogadro's number.

The total heat of the biolayer depends on the amount of DNA molecules, which is related to the packing density and hybridization efficiency. In McKendry's experiments [8], a maximum signal or packing density of 1.3×10^{13} probes/cm^2, was obtained only after 5 min of incubation. The density of probe DNA was unaffected by the salt concentration of the buffer or dilution with ethanol. This value is in agreement with other reports for 12-mers [27,28] and corresponds to 1.5×10^{10} probes/cantilever, where a ssDNA molecule occupies an area of 3.2 nm^2, which approaches the theoretical maximum packing density (this estimate does not take into account the surface roughness of the gold film). The hybridization efficiency is a ratio of the number of bound mol-

ecules to the total number of available binding sites. The hybridization efficiency was reported as 10 % to 100 % for different self-assembly techniques and different reaction conditions [27–29]. However, even for 10 % hybridization efficiency, McKendry et al. [8] predicted that the number of double helices on a tiny reaction area (cantilever dimensions, $500 \times 100\,\mu m^2$) exceeds 10^9. By exact calculations, we obtain that the number of double helices attains 6.5×10^{10}. So, it is necessary to consider the hybridization exothermic effect induced by crowded DNA chains on such a tiny chip.

Next, a description of the hybridization efficiency r will be provided. Assume the target-probe binding events are independent and unaffected by surface coverage, the Langmuir adsorption isotherm states [8] that

$$r = c/(K^{-1} + c), \tag{3}$$

where c is the concentration of target molecules in solution and K^{-1} is the thermodynamic equilibrium dissociation constant related to buffer salt concentrations [8]. So, the total thermal output Q_a of the biolayer can be predicted by

$$Q_a = r\eta S Q_s, \tag{4}$$

in which $S = lb$ is the surface area of the chip and η is the packing density of ssDNA chains. By using Eqs. 1–4 and the related experimental conditions [8], the total thermal output of the biolayer in 1 M NaCl buffer solution is 1 nJ, which might be detectable by a micromechanical sensor with an estimated sensitivity of 1 pJ [30].

The cumulative number of bound molecules was simulated by a first-order chemical reaction equation [16]. An exponential function was obtained for the number of bound molecules. For simplicity, the time history of the hybridization exothermic reaction can also be described as follows:

$$Q(t) = Q_a(1 - e^{-\alpha t}). \tag{5}$$

The experimental data in Refs. [8] and [10] show that the chips can attain steady-state responses after 12 min to 15 min. Assume that 99 % hybridization heat in the biolayer is released when the time $t = 1{,}200$ s, then we obtain $\alpha = 0.004\,s^{-1}$.

2.2 Temperature Field of the Non-biolayers

2.2.1 Three Models for the Temperature Field

Based on Fourier's law, the temperature distribution in the non-biolayers can be predicted by

$$T_{i,t} = k_i T_{i,yy}, \quad i = 1, 2, 3, \tag{6}$$

in which T_i is the temperature. For simplicity, the heat exchange in the biolayer is not considered here. As the heat loss to the surroundings is neglected, the thermal output

of the biolayer is totally transformed into the thermal input of the abiological layers (Au/Ti/Si-layer). So, the boundary condition at the interface between the Au-layer and the biolayer is

$$-\lambda_1 T_{1,y} = \dot{Q}(t)/S, \quad y = 0, \tag{7}$$

The interface continuous conditions are given as

$$T_j = T_{j+1}, \quad \lambda_j T_{j,y} = \lambda_{j+1} T_{j+1,y}, \quad y = \sum_{i=1}^{j} h_i, \quad j = 1, 2, \tag{8}$$

For a thermal conductivity of air much less than that of silicon, the condition at the bottom of the Si-layer is given as

$$T_{3,y} = 0, \quad y = \sum_{i=1}^{3} h_i, \tag{9}$$

The initial temperature of the non-biolayers is assumed to be same to the room temperature, so the initial conditions are as follows:

$$T_i = T_0, \quad t = 0. \tag{10}$$

in which T_0 is room temperature. The governing Eq. 6, the boundary conditions of Eqs. 7 and 9, the continuous conditions of Eq. 8, and the initial conditions of Eq. 10 form the three-layer Au–Ti–Si-beam model.

Considering that the thickness of the Au/Ti-layer is much thinner than that of the Si-layer, the single-layer Si-beam model can be reduced from the three-layer Au–Ti–Si-beam model, Eqs. 6–10:

$$U_{,t} = k_3 U_{,yy}, \tag{11a}$$

$$-\lambda_3 U_{,y} = \dot{Q}(t)/S, \quad y = 0, \tag{11b}$$

$$U_{,y} = 0, \quad y = h_3, \tag{11c}$$

$$U = T_0, \quad t = 0. \tag{11d}$$

Considering the microscale thickness of the chip, the minute-level reaction time, and the good thermal conductivity of metals, the temperature distribution in chips can also be predicted by the following simplified lumped parameter model:

$$\sum_{i=1}^{3} \rho_i c_i h_i \dot{T}(t) = \dot{Q}(t)/S, \tag{12a}$$

$$T = T_0, \quad t = 0, \tag{12b}$$

in which T is the temperature.

2.2.2 Some Analytical Solutions to the Temperature Field

Considering the difficulty of an inverse Laplace transformation, it is impossible to obtain an analytical solution to the three-layer beam model, Eqs. 6–10, by the Laplace transformation method. However, the method of variable separation can be applied to the single-layer beam model, Eqs. 11a–d. For the homogenous conditions, let $\varphi = \xi y^2 + \zeta y$ conform with the boundary conditions, Eqs. 11b, c, i.e.,

$$\varphi_{,y} = \zeta = A\, \mathrm{e}^{-\alpha t}, \quad y = 0, \tag{13a}$$

$$\varphi_{,y} = 2\xi h_3 + \zeta = 0, \quad y = h_3, \tag{13b}$$

in which $A = -Q_{\mathrm{a}}\alpha/(S\lambda)$. From Eqs. 13a, b, one obtains

$$\xi = -A\mathrm{e}^{-\alpha t}/(2h_3), \quad \zeta = A\mathrm{e}^{-\alpha t}, \tag{14a}$$

$$\varphi = -A\mathrm{e}^{-\alpha t} y^2/(2h_3) + A\mathrm{e}^{-\alpha t} y. \tag{14b}$$

Let $V(y,t) = U(y,t) - \varphi(y,t)$, then the following initial-boundary-value problem is given as

$$V_{,t} - k_3 V_{,yy} = A\alpha\mathrm{e}^{-\alpha t} y - A\alpha\mathrm{e}^{-\alpha t} y^2/(2h_3) - Ak_3\mathrm{e}^{-\alpha t}/h_3, \tag{15a}$$

$$V_{,y} = 0, \quad y = 0 \text{ and } h_3, \tag{15b}$$

$$V = Ay^2/(2h_3) - Ay, \quad t = 0. \tag{15c}$$

Let $V(y,t) = v(y,t) + u(y,t)$, where v and u, respectively, are the solutions to the following initial-boundary-value problems:

$$v_{,t} - k_3 v_{,yy} = 0, \tag{16a}$$

$$v_{,y} = 0, \quad y = 0 \text{ and } h_3, \tag{16b}$$

$$v = Ay^2/(2h_3) - Ay, \quad t = 0, \tag{16c}$$

and

$$u_{,t} - k_3 u_{,xx} = A\alpha e^{-\alpha t} y - A\alpha e^{-\alpha t} y^2/(2h_3) - Ak_3 e^{-\alpha t}/h_3, \tag{17a}$$

$$u_{,y} = 0, \quad y = 0 \text{ and } h_3, \tag{17b}$$

$$u = 0, \quad t = 0. \tag{17c}$$

By the method of variable separation, an analytical solution to the problem, Eqs. 16a–c:

$$v(y,t) = \frac{1}{h_3}\int_0^{h_3}\left(\frac{A\xi^2}{2h_3} - A\xi\right)\mathrm{d}\xi + \sum_{n=1}^{+\infty}\frac{2}{h_3}\int_0^{h_3}\left(\frac{A\xi^2}{2h_3} - A\xi\right) \times \cos\frac{n\pi\xi}{h_3}\,\mathrm{d}\xi e^{-k\left(\frac{n\pi}{h_3}\right)^2 t}\cos\frac{n\pi y}{h_3}. \tag{18}$$

Let $u(y,t) = \int_0^t \psi(y,t,\tau)\,\mathrm{d}\tau$, then the problem, Eqs. 17a, b, can be transformed into

$$\psi_{,t} - k_3\psi_{,yy} = 0, \tag{19a}$$

$$\psi_{,y} = 0, \quad y = 0 \text{ and } h_3, \tag{19b}$$

$$\psi = A\alpha e^{-\alpha\tau} y - A\alpha e^{-\alpha\tau} x^2/(2h_3) - Ak_3 e^{-\alpha\tau}/h_3, \quad t = \tau, \tag{19c}$$

By introducing the coordinate transformation $s = t - \tau$, Eqs. 19a–c can be changed into

$$\psi_{,s} - k_3\psi_{,yy} = 0, \tag{20a}$$

$$\psi_{,y} = 0, \quad y = 0 \text{ and } h_3, \tag{20b}$$

$$\psi = A\alpha e^{-\alpha\tau} y - A\alpha e^{-\alpha\tau} x^2/(2h_3) - Ak_3 e^{-\alpha\tau}/h_3, \quad s = 0, \tag{20c}$$

Applying the method of variable separation to the problem, Eqs. 20a–c, one obtains

$$\psi(y,t,\tau)=\frac{1}{h_3}\int_0^{h_3}A\left(\alpha e^{-\alpha\tau}\xi-\frac{\alpha e^{-\alpha\tau}}{2h_3}\xi^2-\frac{k_3e^{-\alpha\tau}}{h_3}\right)d\xi + \sum_{n=1}^{+\infty}\frac{2}{h_3}\int_0^{h_3}A\left(\alpha e^{-\alpha\tau}\xi-\frac{\alpha e^{-\alpha\tau}}{2h_3}\xi^2-\frac{k_3e^{-\alpha\tau}}{h_3}\right) \times\cos\frac{n\pi}{h_3}\xi d\xi e^{-k\left(\frac{n\pi}{h_3}\right)^2(t-\tau)}\cos\frac{n\pi}{h_3}y, \tag{21}$$

Using $u(y,t)=\int_0^t\psi(y,t,\tau)\,d\tau$ and Eq. 21, the solution to the problem, Eqs. 17a, b, is given as

$$u(y,t)=\int_0^t\left[\frac{1}{h_3}\int_0^{h_3}A\left(\alpha e^{-\alpha\tau}\xi-\frac{\alpha e^{-\alpha\tau}}{2h_3}\xi^2-\frac{k_3e^{-\alpha\tau}}{h_3}\right)d\xi + \sum_{n=1}^{+\infty}\frac{2}{h}\int_0^{h}A\left(\alpha e^{-\alpha\tau}\xi-\frac{\alpha e^{-\alpha\tau}}{2h_3}\xi^2-\frac{k_3e^{-\alpha\tau}}{h_3}\right)\cos\frac{n\pi}{h_3}\xi d\xi e^{-k_3\left(\frac{n\pi}{h_3}\right)^2(t-\tau)} \times\cos\frac{n\pi}{h_3}y\right]d\tau, \tag{22}$$

From $U(y,t)=V(y,t)+\varphi(y,t)$, $V(y,t)=v(y,t)+u(y,t)$, and Eqs. 14b, 18, and 22, one obtains

$$U(y,t)=-\frac{Ae^{-\alpha t}}{2h_3}y^2+Ae^{-\alpha t}y+\sum_{n=1}^{+\infty}\frac{2}{h_3}\int_0^{h_3}A\left(\frac{\xi^2}{2h_3}-\xi\right)\cos\frac{n\pi}{h_3}\xi d\xi e^{-k_3\left(\frac{n\pi}{h_3}\right)^2t} \times\cos\frac{n\pi}{h_3}y+\int_0^t\left[\sum_{n=1}^{+\infty}\frac{2}{h_3}\int_0^{h_3}A\left(\alpha e^{-\alpha\tau}\xi-\frac{\alpha e^{-\alpha\tau}}{2h_3}\xi^2-\frac{k_3e^{-\alpha\tau}}{h_3}\right) \times\cos\frac{n\pi}{h_3}\xi d\xi e^{-k_3\left(\frac{n\pi}{h_3}\right)^2(t-\tau)}\cos\frac{n\pi}{h_3}y\right]d\tau, \tag{23}$$

As for the simplified lumped parameter model, Eqs. 12a–c, it is not difficult to obtain its analytical solution as follows:

$$\Delta T=T(t)-T(0)=Q_a(1-e^{-\alpha t})/\left(S\sum_{i=1}^{3}\rho_ic_ih_i\right). \tag{24}$$

Table 2 Physical parameters of the chip

Materials	ρ (kg · m^{-3})	E (GPa)	λ (W · m^{-1} · K^{-1})	α (10^{-6} K^{-1})	k (10^{-6} m^2 · s^{-1})	c (J · kg^{-1} · K^{-1})
Au	19,300	73	315	14.2	130	127
Ti	4,500	106	22	10	9.4	520
Si	2,328	100	150	2.6	92	700

2.3 Deflection of DNA Chip

Based on Zhang's two-variable model for laminated cantilever beams [22–25], the free-end deflection of the chip can be predicted as follows:

$$w = 3l^2\Delta T\{E_2h_2^2[E_1h_1(\alpha_1-\alpha_2)+E_3h_3(\alpha_2-\alpha_3)]+h_2[E_1E_2h_1^2(\alpha_1-\alpha_2)+E_2E_3h_3^2(\alpha_2-\alpha_3)+2E_3E_1h_1h_3(\alpha_1-\alpha_3)]+E_3E_1h_1h_3(h_1+h_3)(\alpha_1-\alpha_3)\}/[E_2^2h_2^4+E_1^2h_1^4+4E_3E_1h_1^3h_3+6E_3E_1h_1^2h_3^2+4E_3E_1h_1h_3^3+E_3^2h_3^4+4E_2h_2^3(E_1h_1+E_3h_3)+6h_2^2(E_1E_2h_1^2+2E_3E_1h_1h_3+E_2E_3h_3^2)+4h_2(E_1E_2h_1^3+3E_3E_1h_3h_1^2+3E_3E_1h_1h_3^2+E_2E_3h_3^3)]. \quad (25)$$

3 Numerical Results

In computation, the physical parameters of the chip are listed in Table 2 [8,10]. The geometrical parameters $l = 500\,\mu\text{m}$, $b = 100\,\mu\text{m}$, $h_1 = 20\,\text{nm}$, $h_2 = 2\,\text{nm}$, and $h_3 = 1\,\mu\text{m}$. The initial temperature $T(0) = 295\,\text{K}$. The other parameters are $\eta = 1.3 \times 10^{17}$ chains · m^{-2}, $c = 1\,\text{M}$, and $K^{-1} = 31 \times 10^{-9}\,\text{M}$.

Based on the three-layer Au–Ti–Si beam model, Eqs. 6–10, the single-layer Si-beam model, Eqs. 11a–d, and the lumped parameter model, Eqs. 12a, b, comparisons of the steady-state temperature change induced by the hybridization exothermic reaction are shown in Table 3. The thiolated probe DNA sequence is ACATTGTCGCAA and its complementary target DNA sequence is TTGCGACAATGT. During calculations, the two-term truncated approximation is taken in the formula, Eq. 23. The DINLAP function in the software of Fortran PowerStation is used for the numerical inverse Laplace transformation. Various predictions based on different models by different methods give almost the same results. This indicates that the lumped parameter model is a good choice for temperature analysis of the chip if the temperature distribution across the thickness can be viewed as homogenous.

The time history of the temperature variation induced by the hybridization exothermic reaction of the above-mentioned DNA sequences is shown in Fig. 2. As a function of time, the temperature variation of the chip approaches its steady-state value of 0.012 K.

Comparisons of the temperature variation and thermal deflection induced by different DNA sequences are shown in Table 4. Obviously, the temperature variation and the thermal deflection enhance with the increase of GC base pairs. During the DNA hybridization process, the temperature rise of the chip is of the order of 10^{-2} K, and

Table 3 Steady-state temperature change of the chip

Model	Temperature change (K)
Single-layer model (variable separation method)	0.0120395
Single-layer model (Laplace transformation method)	0.0120390
Three-layer model (Laplace transformation method)	0.0121630
Lumped parameter model	0.0119148

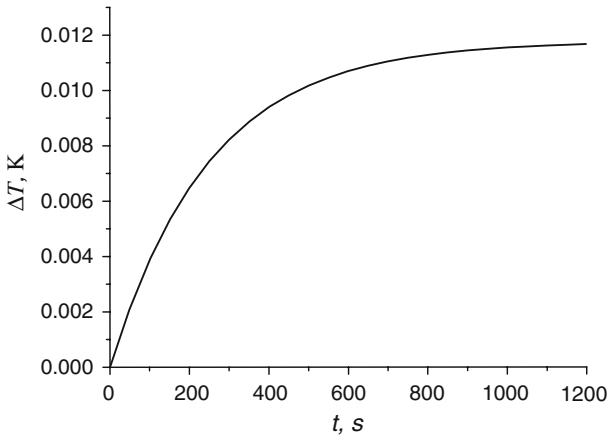

Fig. 2 Time history of temperature variation of the chip

the thermal deflection is 1.5 nm to 2 nm, which is consistent with 0.5 nm deflection estimated for a micromechanical sensor caused by the reaction heat [31]. McKendry et al. [8] pointed out that the uncertainty of the optical-beam-deflection readout system has reached the order of 0.1 nm. And experimental studies [5] showed that the differential deflection induced by mismatches at internal, distal, and proximal locations on the complementary strand is only 1 nm to 4 nm. So, we believe that a deflection of the order of 1.5 nm to 2 nm might be detected by the readout system. The present prediction of thermal deflection is about 15 % of the total hybridization deflection, which might be a little higher than the experimental values because the heat loss to the surroundings is neglected. However, the result will help to reconsider detection of the time span because fast response is one of the claimed merits for this new label-free technology. It is advisable to detect nanomechanical deflections of the chip after the reaction system is sufficiently cooled.

4 Conclusions

A simple mathematical model is provided for temperature variations and sequence-dependent nanomechanical deflections of DNA chips induced by the hybridization exothermic effect. In label-free biodetections, if the heat loss to the surroundings is

Table 4 Temperature change and thermal deflection induced by DNA hybridization

Probe DNA sequence	Temperature variation (K)	Free-end deflection (nm)
ACA TTG TCG CAA	0.012	1.66362
TGC TGT TTG AAG	0.011	1.52499
CCG GAA GAT TGC	0.014	1.94089
GGA AGC CGA GCG	0.015	2.07953

neglected, the total thermal output of the biolayer is about 1 nJ, the temperature rise of the chip is 10^{-2} K, and the thermal deflection is 1.5 nm to 2 nm, which might be detected by the optical-beam-deflection readout system. One should be careful to control the detection time if more precise requirements are needed.

Acknowledgments The research was sponsored by the Multiscale Material Mechanics Fellowship, the Natural Science Foundation of Shanghai Municipality (No. 07ZR14037), the Research Innovation Program of Shanghai Education Commission (No. 09YZ07), the Natural Science Foundation of China (10872121), the Shanghai Leading Academic Discipline Project (No. Y0103), the National Outstanding Young Scientists Foundation of China (No. 10725209), and the Graduate Student Innovation Foundation of Shanghai University (No. SHUCX080223).

References

1. N.H. Zhang, J.Y. Shan, J. Mech. Phys. Soilds **56**, 2328 (2008)
2. N.H. Zhang, J.Y. Shan, J.J. Xing, Acta Mech. Solida Sin. **20**, 206 (2007)
3. N.H. Zhang, J.J. Xing, J.Y. Shan, in *Proceedings of 5th International Conference on Nonlinear Mechanics*, ed. by W.-z. Chien, S.-q. Dai, Z.-w. Zhou, C.-j. Cheng (Shanghai University Press, Shanghai, 2007), p. 562
4. J.C. Stachowiak, M. Yue, K. Castelino, A. Chakraborty, A. Majumdar, Langmuir **22**, 263 (2006)
5. K.M. Hansen, T. Thundat, Methods **37**, 57 (2005)
6. M. Alvarez, L.G. Carrascosa, M. Moreno, A. Calle, A. Zaballos, L.M. Lechuga, A.C. Martinez, J. Tamayo, Langmuir **20**, 9663 (2004)
7. F. Liu, Y. Zhang, Z.C. Ou-Yang, Biosens. Bioelectron. **18**, 655 (2003)
8. R. McKendry, J.Y. Zhang, Y. Arntz, T. Strunz, M. Hegner, H.P. Lang, M.K. Baller, U. Certa, E. Meyer, H.J. Guntherodt, Ch. Gerber, Proc. Natl. Acad. Sci. U.S.A. **99**, 9783 (2002)
9. G.H. Wu, H.F. Ji, K.M. Hansen, T. Thundat, R. Datar, R. Cote, M.F. Hagan, A.K. Chakraborty, A. Majumdar, Proc. Natl. Acad. Sci. U.S.A. **98**, 1560 (2001)
10. J. Fritz, M.K. Ballar, H.P. Lang, H. Rothuizen, P. Vettiger, E. Meyer, H.J. Guntherodt, Ch. Gerber, J.K. Gimzewski, Science **288**, 316 (2000)
11. M. Yue, H. Lin, D.E. Dedrick, S. Satyanarayana, A. Majumdar, A.S. Bedekar, J.W. Jenkins, S. Sundaram, J. Microelectromech. Syst. **13**, 290 (2004)
12. S. Jeon, N. Jung, T. Thundat, Sens. Actuators B **122**, 365 (2007)
13. L.G. Carrascosa, M. Moreno, M. Alvarez, Trends Anal. Chem. **25**, 196 (2006)
14. M.R. Begley, M. Utz, U., Komaragiri, J. Mech. Phys. Solids **53**, 2119 (2005)
15. R.B. Meyer, Phys. Rev. Lett. **22**, 918 (1969)
16. A.-R.A. Khaled, K. Vafai, M. Yang, X. Zhang, C.S. Ozkan, Sens. Actuators B **94**, 103 (2003)
17. P.G. Datskos, N.V. Lavrik, S. Rajic, Rev. Sci. Instrum. **75**, 1134 (2004)
18. A.N. Cleland, M.L. Roukes, J. Appl. Phys. **92**, 2758 (2002)
19. K.J. Breslauer, R. Frank, H. Blöcker, L.A. Marky, L.A., Proc. Natl. Acad. Sci. U.S.A. **83**, 3746 (1986)
20. J.A. Holbrook, M.W. Capp, R.M. Saecker, M.T. Record, Biochemistry **38**, 8409 (1999)
21. M.F. Hagan, A. Majumdar, A.K. Chakraborty, J. Phys. Chem. B **106**, 10163 (2002)
22. N.H. Zhang, J.Z. Chen, ASME J. Appl. Mech. **75**, 044503 (2008)
23. N.H. Zhang, Thin Solid Films **515,** 8402 (2007)

24. N.H. Zhang, J.J. Xing, J. Appl. Phys. **100**, 103519 (2006)
25. N.H. Zhang, J.Z. Chen, Euro. J. Mech. A/Solids, doi:10.1016/j.euromechsol.2008.07.004 (2008)
26. Z.C. Zheng, Chem. Life **21**, 254 (2001) (in Chinese)
27. T.M. Herne, M.J. Tarlov, J. Am. Chem. Soc. **119**, 8916 (1997)
28. A.B. Steel, R.L. Levicky, T.M. Herne, M.J. Tarlov, Biophys. J. **79**, 975 (2000)
29. R. Levicky, T.M. Herne, M.J. Tarlov, S.K. Satija, J. Am. Chem. Soc. **120**, 9787 (1998)
30. J.K. Gimzewski, Ch. Gerber, E. Meyer, R.R. Schlittler, Chem. Phys. Lett. **217**, 589 (1994)
31. R. Berger, E. Delamarche, H.P. Lang, Ch. Gerber, J.K. Gimzewski, M. Meyer, H.-J. Güntherodt, Science **276**, 2021 (1997)